The plasmasphere of Neptune

Tian-Sen Huang and C. Wing Ho

Department of Physics, Prairie View A&M University, Prairie View, Texas

Claudia J. Alexander

Jet Propulsion Laboratory, Pasadena, California

Abstract. We examine the plausible existence of **Neptune**'s **plasmasphere** and study the drift of particles inside it. Using the O8 **magnetic field** model [*Connerney et al.*, 1991] and assuming a uniform **solar wind** convection electric field, the plasma convection time and refilling time are calculated in a Euler potential coordinate system [*Ho et al.*, 1997]. The plasma density and refilling time at the equilibrium state are first calculated, and the location of the plasmapause is set to be where the refilling time and convection time are equal. The refilling time as a function of ion speed is then recalculated along field lines, and the plasma density and temperature are obtained by directly integrating the local ion distribution function over the range of speeds for which the refilling time is less than the convection time. The density calculated using this model shows sharp drop-offs at approximately 3.25 to 4.5 R_N on the zero magnetic scalar potential surface, a boundary taken to be the plasmapause. Our calculated density compares fairly with the observed density along the **Voyager** trajectory within about 5 R_N. Ion temperature is also calculated along the field line with results which indicate that high-speed tails of the distribution function might be needed to explain the high observed temperature measured along the Voyager 2 trajectory. Drift trajectories and speeds of 90° pitch angle particles inside the plasmapause are calculated. Particles of energy above tens of eV are gradient drift dominated, and the drift paths of this class of particles are essentially the minimum B contours that are similar to *Acuña et al.*'s [1993] calculations. Atmospheric precipitation of the $J = 0$ particles may provide an explanation for the UV emissions, as an alternative to the "monoprecipitation" suggested by *Paranicas and Cheng* [1994]. Drifts of low-energy particles are strongly affected by the gravitational and centrifugal forces, and because of the largely tilted dipole and the large higher components of magnetic field, the resultant drift is nonaxisymmetric and quite complicated.

1. Introduction

Due to the superposition of the solar wind driven convection electric field and the planetary corotation electric field, there exists a region near Earth where the electrical equipotentials on the

equatorial plane are closed contours [*Kavanagh et al.*, 1968]. This region also marks the particle streamline contours and defines to a first approximation the plasmasphere of the planet [*Nishida*, 1966; *Brice*, 1967]. These statements are true for the ideal case in which the planetary rotation axis and magnetic dipole axis are aligned, and the rotation axis is perpendicular to the solar wind flow direction. Good approximations to the ideal case can be made for planets such as Earth, Jupiter, and Saturn, and the sizes of the plasmaspheres of these planets have been estimated in such manner. For Neptune, which has its relative orientations of rotation axis, magnetic dipole axis, and solar wind flow direction deviate grossly from the ideal case, the existence of a plasmasphere is not so readily determined.

Selesnick and Richardson [1986] studied the plausible formation of plasmaspheres in an arbitrarily oriented magnetosphere and concluded that a planet whose rotation axis makes an angle θ_S with the solar wind flow direction and θ_D with the dipole axis can form a plasmasphere only in the cases of $\theta_D = 0°$ or $\theta_S = 90°$. In the first case, the dipole field lies along the rotation axis and maintains a constant angle with the solar wind flow, where a steady plasmasphere exists. In the latter case, because of the constant change of the dipole axis relative to the solar wind flow, the convection electric field is time dependent and the particle trajectories do not form closed paths but are bounded due to symmetry, so a plasmasphere still exists but varies with time. There is another special case in which $\theta_S = 0°$ and θ_D is arbitrary, i.e., the rotation axis is solar wind flow aligned, in which case corotation does not produce a closed flow to impede the solar wind driven convection, so the magnetosphere is convection dominated and no plasmasphere exists [*Vasyliunas*, 1986; *Selesnick and Richardson*, 1986]. When neither of the above cases are true but the rotation and dipole axes are oriented arbitrarily, the time dependence of the electric field and the lack of symmetry of the system make it difficult to locate a plasmasphere, if it exists, simply by comparing the relative contributions of the corotation field and convection field as in the usual manner. Such is the case for the planet Neptune.

According to *Ness et al.*'s [1989] OTD (Offset Tilted Dipole) model, Neptune has a dipole axis tilted about 47° from the rotation axis. Together with the 113° angle the rotation axis made

with the Neptune-Sun direction during the Voyager 2 flyby to the planet, the large tilted angle results in an "Earth-like" and a "pole-on" magnetic field configurations at two extreme positions during each revolution of the planet as the rotation axis, the dipole axis and the Neptune-Sun direction all lie in the same plane [*Ness et al.*, 1989; *Selesnick*, 1990]. These two extreme positions represent the upper and approximately the lower limits of the efficiency of coupling between the solar wind and the convection over the polar cap, and the strong modulation of the convection electric field in the Neptunian magnetosphere causes a cumulative effect like the acceleration of particles in a cyclotron [*Selesnick*, 1990].

Since Neptune has an Earth-like position and Earth has a plasmasphere, and while in the pole-on position, solar wind magnetosphere coupling at Neptune is the weakest and the likelihood to form a plasmasphere is highest, Neptune should also have a plasmasphere. The existence of a plasmasphere at Neptune is also supported by the Voyager 2 Plasma Wave Instrument (PWS), which detected whistler signals with large dispersions [*Gurnett et al.*, 1989] that require dense plasma path lengths along field lines.

Further arguments for the existence of a Neptunian plasmasphere can be made as follows: Neptune has a region, extended to about three planetary radii (1 R_N = 24,765 km), dominated by the gravitational force, and in this region the ionospheric plasma refilling surpasses the solar wind driven convection. *Lemaire* [1974] has used the critical distance, "Roche Limit," beyond which the refilling time quickly increases, to define Earth's plasmapause. Earth's plasmasphere defined in this way has a size of 5.8 R_E, a value not too far from the actual observed average values. For Neptune, assuming a spin axis-aligned dipole as a rough estimate, the critical distance of Neptune is 3 R_N. However, because of the larger gravity and the lower ionospheric temperature of Neptune [*Tyler et al.*, 1989], the plasma distribution in the plasmasphere differs from that of the terrestrial plasmasphere in that the plasma density gradient along a field line from the ionosphere to the equatorial plane is quite large. As a result of the low plasma density of ionospheric origin along the field line in the low magnetic latitude region, the increase of plasma refilling time with increasing L

shell is not so fast as in the terrestrial magnetosphere, and hence the actual size of the Neptunian plasmasphere might be larger than the above estimated of 3 R_N.

In this paper, based on the competition of plasma refilling with the solar wind driven convection, we construct a model of plasmasphere at Neptune. We also study the particle drift motions inside the plasmasphere. The magnetic field model we use for various calculations is the O8 model [*Connerney et al.* 1991], and for representing it the α and β (Euler potentials) coordinates [*Ho et al.*, 1997] are used. The O8 model, including the dipole, quadrupole and octupole of the field, has been used to study field geometry invariants and drift shells [*Acuña et al.*, 1993], and aurora in association with UV emissions [*Paranicas and Cheng*, 1994].

This paper is structured as follows. In section 2, we calculate the plasma density originating from the ionosphere, assuming an equilibrium state, i.e., a full Maxwellian distribution everywhere on the concerned field lines. We then proceed by comparing the solar wind driven convection time with the plasma refilling time to estimate the size of the plasmasphere, as an approximation. Next, for a more accurate calculation, we consider the local dynamic accessibility of particles in the refilling process. This is followed by a more meticulous study of the dynamics of ions along the field lines. To do this, we calculate the refilling time of the ions that can access a certain point on a field line. By integrating the local ion distribution function over the range of ion speeds that correspond to a refilling time less than the convection time, the ion density and temperature can be obtained. The location of the plasmapause is thus determined to be where the densities show sudden drop-offs. In section 3, we compare the calculated plasma densities and temperatures with the Voyager Plasma Science Experiment (PLS) measurements. In section 4, we calculate the particle drift paths and drift velocities inside the plasmasphere of Neptune. Finally, discussion and conclusions are given in section 5.

2. Formation of Neptune's Plasmasphere

2.1. Equilibrium State Approximation

As an approximation, we assume that the plasma inside Neptune's plasmasphere is in an equilibrium state along the field lines in relative to the ionospheric plasma like that of Earth, but the plasmapause is located at the position where the plasma refilling time is equal to the solar wind driven convection time. Before locating the plasmapause, we first calculate the density of the ionosphere-originated plasma in Neptune's magnetosphere in the absence of the solar wind driven convection.

For a two-species plasma in its equilibrium state, the density along a field line has the familiar form of the exponential dependence on the total potential energy [*Huang and Birmingham*, 1992]. In the presence of gravitational, centrifugal and polarization electrical potential, the density of an isotropic plasma of mass m at position r is

$$n = n_i \exp\left\{\frac{1}{2kT_o}\left[mMG\left(\frac{1}{r}-\frac{1}{r_i}\right)+\frac{1}{2}m\Omega^2\left(\rho^2-\rho_i{}^2\right)\right]\right\} \tag{1}$$

where M is the mass of Neptune (1.0247×10^{26} kg), Ω is the angular rotation frequency (the rotation period of Neptune is 16.11 hours), and ρ is the cylindrical distance from the spin axis. The density given by (1) is expressed relative to the density at the foot points of the field line (subscripts i for N and S represent the north or south end of the field line). Here we assume an isotropic Maxwellian plasma of temperature T_o in the ionosphere (1000 K [*Tyler et al.*, 1989]). The first factor 1/2 of the exponent in (1) is the result of the polarization electric potential, which in a singly charged equilibrium plasma is equal to minus half the sum of the gravitational and centrifugal potential.

It is readily seen that the densities n_N and n_D are related by

$$n_N = n_S \exp\left[\frac{m\Omega^2}{4kT_o}\left(\rho_N{}^2-\rho_S{}^2\right)\right] \tag{2}$$

Owing to the lack of information on the density distribution in the ionosphere, we assume

$$\sqrt{n_N n_S} = n_o \tag{3}$$

where n_o is the density in the ionosphere taken to be uniformly equal to 1000 cm^{-3} [*Tyler et al.*, 1989]. It should be pointed out that (1) can only enable us to calculate the density along each field line, and the resulting plasma density comes from an aggregate of the calculations for each magnetic flux tube.

Figure 1 shows the relative orientations of Neptune's rotation axis Ω, dipole axis **M**, and the solar wind flow direction $\mathbf{v}_{SW}$ adopted from *Selesnick and Richardson* [1986], and the coordinate system upon which all our subsequent three-dimensional plots are based. The set of *xyz* axes makes up what we call the rotation frame, in which the *x* axis is along the 0° West longitude (in the Neptune longitude system adopted by the Voyager Project Steering Group).

The plasma density in equilibrium state calculated from (1), (2), and (3) is shown on the cross sections along field lines in Plate 1a and on the zero magnetic scalar potential surface in Plate 1b. The zero scalar potential surface is everywhere perpendicular to the field lines and lies in close proximity to the minimum *B* surface for $r > 2\ R_N$ [*Ho et al.*, 1997]. The cross sections in Plate 1a are actually the four surfaces of constant Euler potential β of values 0, $\pi/2$, π and $3\pi/2$ (The values of β are equal to the azimuthal angle in radians in the dipole frame for a dipole at large radial distances where dipole field is a good approximation. For details on the definitions of the dipole frame and the values of α and β, (see *Ho et al.* [1997].) Also shown in Plates 1a and 1b are the lines of constant α and β on the zero magnetic scalar potential surface. The lines of constant α take the form of closed rings circling the center, and the lines of constant β resemble spokes of a wheel. Field lines (white solid lines on the constant β surfaces) are also shown in Plate 1a. The color contours on the zero magnetic scalar potential surface in Plate 1b indicate that the density falls off rapidly with distance within 3 to 4 R_N due to the gravitational force, and rises at larger distances

due to the centrifugal force. The distorted magnetic field lines and plasma distribution near the planetary surface are shown very clearly.

Figure 2 shows the potential energies and densities on the zero magnetic scalar potential surface plotted against radial distance at 0°W and 90°W. The gravitational potential (crosses) increases with r, while the centrifugal potential (triangles) decreases with r. The sum of these potentials (circles) has a peak around 3 – 4 R_N. The polarization electrical potential (squares) acts to reduce the potential barrier set up by the gravitational and centrifugal forces. The total potential is shown by the thick solid line, and the plasma density by the thin solid line. The large tilted dipole axis gives rise to the larger (more negative) centrifugal potential near 0°W and 180°W than at 90°W and 270°W, and together with the warped magnetic scalar potential surface result in a nonsymmetrical plasma density distribution. The local density minimum (purple) on the zero magnetic scalar potential surface (Plate 1b) is a result of the combination of the gravity and the centrifugal force of the planet; otherwise, the gravity alone would make it symmetrical about the dipole axis. At sufficiently large distances, due to the tilted dipole axis, the centrifugal force results in a higher density at the upper portion of the field lines around 90°W (the bottom leaf of density cross sections in Plate 1a), and a higher density at the lower portion of the field lines around 270°W (the top leaf of the density cross sections in Plate 1a).

Next we calculate the location of the plasmapause. In this approximation, the plasmapause is taken to be where the solar wind driven convection time and the plasma refilling time are equal. To calculate the convection time, we first determine the solar wind driven $\mathbf{E} \times \mathbf{B}$ drift velocity

$$\mathbf{v}_c = \frac{\mathbf{E}_c \times \mathbf{B}}{B^2} \tag{4}$$

with the expression for the convection electric field $\mathbf{E}_c$ given by

$$\mathbf{E}_c = -E_o \hat{\mathbf{v}}_{SW} \times \hat{\mathbf{M}} \tag{5}$$

The magnitude of $\mathbf{E}_c$ is a maximum of 0.01 mV/m [*Selesnick*, 1990], and due to rotation it is modulated by $\hat{\mathbf{v}}_{SW} \times \hat{\mathbf{M}}$, where $\hat{\mathbf{v}}_{SW}$ and $\hat{\mathbf{M}}$ are the unit vectors of the solar wind and Neptune's magnetic dipole. The timescale for solar wind driven convection of the plasmaspheric plasma at r can be estimated by

$$t_c = \frac{\Delta r}{v_c} \tag{6}$$

where Δr is the scale length at which the effect of convection on the formation of the plasmasphere is significant. For a plasmasphere scaled several R_N, we take Δr to be 0.3 R_N, a fraction of its size.

The refilling time in the case of a nontilted planetocentric dipole has been calculated by *Lemaire* [1985]. For a nonsymmetric field, the refilling time for a flux tube (from empty to the equilibrium state) can be written as

$$t_f = \left(\frac{F_N^{\parallel}}{B_N^r} + \frac{F_S^{\parallel}}{B_S^r} \right)^{-1} \int_N^S \frac{n}{B} ds \tag{7}$$

where B_N^r and B_S^r are the radial components of the magnetic field at the northern and southern ends of the field line, respectively, and $F_N^{\parallel}$ and $F_S^{\parallel}$ are the plasma fluxes flowing out of the topside ionosphere along the field line expressed by

$$F_i^{\parallel} = \frac{1}{4} n_i \sqrt{\frac{8kT_o}{\pi m}} \tag{8}$$

(subscript i represents N and S). By setting the convection time (6) and the plasma refilling time (7) to be equal, the plasmapause is marked out on the zero magnetic scalar potential surface (Plate 1b). Here we show only two extreme cases: one is the pole-on position in which $\mathbf{E}_c$ is a minimum of magnitude 0.0035 mV/m and the plasmapause is slightly larger indicated by crosses; the other case is the Earth-like position in which $\mathbf{E}_c$ is the maximum 0.01 mV/m and the plasmapause is

slightly smaller indicated by solid circles. The plasmasphere boundaries for the two extreme cases are not very much different; both are roughly at 7 R_N. The timescale at this distance is about 2 to 3 days, in rough agreement with the transport time calculated from the magnetosphere input power requirement for a coupling efficiency of 0.1 [*McNutt et al.*, 1987]. In addition, the insensitivity of the calculated plasmapause to the strength of the convection field justifies the use of a steady state model for an otherwise highly dynamic plasmasphere in terms of the constant change in electric fields produced by the interaction of the solar wind with a rotating tilted dipole field.

2.2. Effect of Ionospheric Ion Dynamic Accessibility

In this subsection, we calculate the density and temperature of Neptune's plasmaspheric plasma in a more rigorous manner. In the new calculation, we include the effect of local accessibility of ions due to both the potential energy barriers and the refilling time relative to the convection time. This effect was ignored in the previous equilibrium state approximation.

For a planet that has a spin axis-aligned dipole magnetic field, the total (gravitational, centrifugal, and polarization electric) potential energy of an ion along a field line has a maximum at the magnetic equator for small L shells. For large L shells, there are two maximum potentials along the field line, which are situated on the opposite sides of the equatorial plane. For planets with tilted magnetic dipole and large nondipole components like Neptune, the two potential barriers are located asymmetrically about the magnetic equator. In any case, in order to reach a point on a field line beyond the potential barriers, an ion of ionospheric origin must have enough kinetic energy to overcome the potential barriers, and the ions that can cross over the potential barriers have a nonzero lower velocity cutoff.

Assuming an upward flow of Maxwellian distributed ions from the two hemispheres and using Liouville's theorem to determine the local ion distribution function, the ion densities and temperatures along the field line can be calculated by integrating the local distribution function with the lower cutoff speed. Figure 3 shows the calculated densities (squares) and temperatures (crosses) along a field line at about 0°W that has a maximum radial distance 8 R_N. Tracing from one end of the field to another, one can find two local minimum densities located approximately at

the potential barriers P1 and P2. For comparison, the same quantities from the equilibrium state approximation are also shown in the same figure by the thin solid line (density) and thick line (temperature). In the latitudinal range between 10°N and 50°S, the potential barriers reduce the densities by almost a factor of 10 and increase the temperature by several times.

Besides the potential energy barriers, the solar wind driven convection imposes another dynamic accessibility limit on the ion refilling. The latter limits the ions to refill a section of flux tube to those that have a refilling time smaller than the convection time. To take the convection time into account, we devise a model in which the plasmasphere is filled by the ionospheric ions distributed uniformly in an upper half of a spherical thin shell in velocity space. The refilling starts from the ionosphere followed by the lower portion of the flux tube and moves gradually upward with time. Ions that have refilling time longer than the convection time are excluded.

Following this scheme, we now determine the cutoff speed for a given point on a field line. Later on, the local plasma density and temperature will be calculated by integrating the local ion distribution function using this lower cutoff speed for all accessible ions. The ionospheric ions distributed in the velocity hemispherical shell between v_o and v_o+dv_o have an upward flux

$$F_o = dn_o \bar{v}_o \tag{9}$$

where dn_o is the number density of ions contained in the hemispherical shell, and $\bar{v}_o$ is the average upward velocity given by

$$\bar{v}_o = \frac{v_o}{2} \tag{10}$$

For simplicity, we assume the ions everywhere along the flux tube are quickly isotropized once the ions arrive at a point. This is obviously an oversimplification, but it has been shown that in Earth's plasmaspheric flux tubes, even Coulomb collision alone is an adequate refilling agent, and

isotropization is achieved in less than a hundred hours [*Wilson et al.*, 1992], which is less than the convection time we calculated for the regions we are interested in.

By equating the number of ions flowing from the ionosphere and the number of ions filled in the flux tube of unit base area during the same time, we obtain

$$F_o \sin \psi t = \int_{s_o}^{s} \frac{B_{or}\, dn}{B} ds \tag{11}$$

where ψ is the ionospheric dip angle of the field line, dn is the local ion number density on the field line, B is the magnetic field intensity, B_{or} is the magnetic field radial component at the ionosphere, and s_o is the position of the field line at the ionosphere. From (9), (10), and (11), we obtain the time for the ionospheric ions of velocity v_o to reach a point of interest indicated by s

$$t = \frac{4B_o}{v_o^2} \int_{s_o}^{s} \frac{v}{B} ds \tag{12}$$

where B_o is the magnetic field intensity at the ionosphere. One should bear in mind that this refilling time is a function of v_o and v (v is the ion speed at s which corresponds to v_o at s_o). From the conversation of total energy, v_o and v are related by

$$\frac{mv^2}{2} - \frac{GmM}{r} - \frac{m\Omega^2\rho^2}{2} + q\Phi = \frac{mv_o^{\,2}}{2} - \frac{GmM}{r_o} - \frac{m\Omega^2\rho_o^{\,2}}{2} + q\Phi_o \tag{13}$$

and

$$v dv = v_o dv_o \tag{14}$$

where Φ_o and Φ are the polarization electrical potential at s_o and s, respectively, and can be determined using the density expression for electrons

$$n = n_o \exp\left[\frac{q(\Phi-\Phi_o)}{kT_o}\right] \tag{15}$$

Figure 4 shows some typical variations of t with v. Case A shows that ions of minimum local speed v_{min} have a refilling time t (from s to s_o) shorter than the convection time t_c. The minimum speed v_{min} is the speed of an ion that has just enough energy to cross over the lower of the two potential barriers discussed in the previous section. The minimum speed is equal to zero if there is only one maximum potential along the field line. Case B shows that ions of v_{min} have a refilling time longer than the convection time.

Case A-1 represents the case in which all ions that have overcome the minimum potential barrier arrive at the point of interest in a time less than the convection time. Because of the dependence of t on v, ions of a certain range of speed that require a time in excess of the convection time to arrive locally are inaccessible to the local region, which is shown as Case A-2. Case A-2 represents the most interesting case in which the ions form two groups: a group of small-velocity ions and a group of large-velocity ions. The large-velocity ions form the tail of the distribution and the resultant temperature is high. The contribution from the high- temperature tails in our case is found to be insignificant, so the resultant temperatures are rather low (a fraction of the equilibrium temperature of 1000°K). If only ions from the high-speed tail were able to cross over the potential barriers (Case B-1), they would form a low-density, high-temperature ion population. Nevertheless, Case A-2 can yield a high resultant temperature as well if the low temperature portion is small enough and the high-speed tail has a reasonably high density. The temperatures are very sensitive to the cutoff speeds for Case A-2.

The density and temperature at s are now calculated by integrating the ion distribution function for all accessible ions. Assuming a Maxwellian distribution of ions in the ionosphere and using Liouville's theorem, the density n and temperature T at s are given by

$$n = 4\pi C \int_{v_{min}}^{\infty} \exp\left(\frac{-mv_o^2}{2kT_o}\right) v^2 dv \tag{16}$$

$$\dot{T} = \frac{4\pi mC}{3kn}\int_{v_{min}}^{\infty} \exp\left(\frac{-mv_o^2}{2kT_o}\right) v^4 dv \qquad (17)$$

where $C = n_o(m/2\pi kT_o)^{3/2}$. The integration is carried out over all ions that have speed above v_{min} but precludes those which have a refilling time longer than the convection time.

In calculating the density on the zero scalar potential surface as in the previous section, we find that the densities drop off quite rapidly within a small range of r. The locations of the sharp density drop-offs are a more accurate estimate of the plasmapause. The newly calculated plasmapause is located in a range of 3.25 to 4.5 R_N (indicated by the asterisks in Plate 1b).

3. H^+ Densities and Temperatures Along the Voyager 2 Trajectory

In this section, we compare our results with the Voyager 2 PLS data. The densities calculated in the equilibrium state are plotted versus r (squares) in Figure 5. This figure also shows the observed H^+ densities (dots) with 1 σ error bars [*Richardson et al.*, 1991]. Along both the inbound and outbound of Voyager 2, the calculated H^+ densities fall off rapidly with r for $r \leq 3$ R_N, and increase rapidly with r beyond that. The rapid increase and then decrease of density with r are, as have been discussed earlier, due to the dominant gravitational force near the planet and the increase of centrifugal force with increasing distance from the spin axis. Along the inbound trajectory, very few data are available between 4 and 5 R_N as well as inside 2.5 R_N due to low flux levels. Overall, the Voyager measurements inbound are below the calculated densities. The measured densities outbound are lower than the calculated densities inside 2.5 R_N and higher from 2.5 to 3.5 R_N; nevertheless, they follow the same trend of a rapid falloff of density with distance in this region where gravity is dominant.

For particles that are still in the equilibrium state, but excluding those which could not cross the potential barrier, the results are shown as circles in Figure 5. Below a distance of approximate 3 R_N, ions of all speeds are accessible to the points on the Voyager 2 trajectory. The calculated

densities are therefore of no difference from the previous calculations (squares). Above about 3 R_N, the exclusion of some low-speed ions results in smaller densities.

Finally, the densities for the ions that can both cross the potential barriers and have refilling time smaller than the convection time are recalculated and are shown as triangles in Figure 5. The density drops drastically along the Voyager 2 trajectory both inbound and outbound. The drop in density is due to the exclusion of those ions that have a refilling time longer than the convection time. The sharp density discontinuity indicates the position of the plasmapause at about 2.5 R_N inbound and 3.5 R_N outbound. As the spacecraft flew inbound and outbound, it encountered ions with the distribution function shown in Figure 4 (Figure 4 is actually not the ion distribution, but viewing it as such facilitates the discussion here). The corresponding cases shown in Figure 4 are displayed in Figure 5 as follows: Case A-1 corresponds to where the circles and the triangles overlap, i.e., the bulk of the plasma inside the plasmasphere; Case A-2 corresponds to the rest of the open triangles; and Case A-3 corresponds to the solid triangles.

The measured densities at about 3 R_N inbound, about 0.03 cm^{-3}, are within the range we calculated. Outbound at about 4 – 5 R_N the measured densities are higher than the calculated densities, while at less than 2 R_N the measured densities are lower than the calculated densities. It should be pointed out that the Voyager 2 PWS measured whistler waves with large dispersion that suggest higher ion densities than were obtained by the PLS instrument. The calculated density drop-off is at a smaller radial distance inbound because Voyager 2 approached Neptune at a larger L shell than outbound (see, for example, Figure 7 of *Richardson et al.* [1991]). The regions around 3 R_N inbound and 4 – 5.5 R_N outbound are where our calculation indicates a sharp drop-off in density, which are also where low densities are observed, we conclude that these are the edges of the plasmasphere. Beyond the plasmapause, no ions of ionospheric source are found; this is represented by Case B-2. However, we should bear in mind the existence of plasmas from other sources such as the moons and the rings.

We can also integrate the distribution function using (17) to obtain the ion temperatures which are plotted in Figure 6 (circles). The ion distribution function that has a nonzero cutoff speed

yields a temperature that is higher than the equilibrium temperature of 1000°K. As we mentioned earlier, Case B-1 potentially yields an ion plasma population of high temperature. In order to show the high temperature, a high- speed tail is needed. Temperatures calculated using only the high-speed tail of the ions are plotted in Figure 6 (triangles). Case A-2 represents the case in which the temperatures are potentially high; it is probably mixed with ions of Case B-1. The observed high temperature in the range of 3 – 4 R_N might correspond to ions of these two cases. The plasma temperatures calculated here did not include other possible processes of heating such as wave-particle interactions, frictional heating, and other microscopic processes.

4. Particle Drifts Inside the Neptune Plasmasphere

In this section we calculate the particle drift paths and drift velocities inside the plasmasphere. Here only particles with 90° pitch angle are considered; these are particles which have no bounce motion alone the field line, and therefore have zero second adiabatic invariant ($J = \int m v_{\|} ds = 0$). This class of particles does not form drift shells as particles of pitch angles less than 90° do. In the absence of bounce motion, the drift velocity of a particle due to the gradient of magnetic field and the gravitational, centrifugal and polarization electrical forces is given by

$$\mathbf{v}_d = \frac{\mu}{q}\frac{\mathbf{B}\times\nabla\mathbf{B}}{B^2} + \frac{1}{qB^2}\left[-\frac{mMG}{r^3}\mathbf{r} - m\boldsymbol{\Omega}\times(\boldsymbol{\Omega}\times\mathbf{r}) - \nabla\Phi\right]\times\mathbf{B} \qquad (18)$$

where μ is the first adiabatic invariant of the particle. *Gao et al.* [this issue] have shown that $J = 0$ particles drift from one field line to another maintaining μ maximum on each field line. They also pointed out that the drift velocity $\mathbf{v}_d$ given in (18) is only the component of the actual drift velocity $\mathbf{u}$ perpendicular to the field line. The actual drift velocity includes a component parallel to the field line contributed by a small parallel velocity $\mathbf{v}_{\|}$. (Note: $J = 0$ still holds.) The magnitude of the actual drift velocity is given by

$$u = \frac{v_d}{\cos\xi} \qquad (19)$$

where ξ is the angle between $\mathbf{u}$ and $\mathbf{v}_d$.

Plate 2 shows the drift paths of particles of total energy 1 eV, which are the contours of μ on a surface made up of the maximum μ on each field line. The drift paths mostly encircle the planet at $r > 2\ R_N$; the twisted drift paths (marked O next to it) are due to the severely distorted magnetic field structure in this region. Very near the planet (~1.5 R_N), some of the drift paths converge to the planet's surface. These ions enter the neutral atmosphere and may cause the UV emissions that were observed by the Voyager 2 UVS instrument. Three such regions into which the drift paths converge are indicated by I, II, and III in Plate 2, approximately at 180°W, 15°W, and 135°W. All three regions are at longitudes which coincide with some of the "monoprecipitation" due to weak-B footprints of monotonic field lines on the planetary surface [*Paranicas and Cheng*, 1994]. General precipitation of this type also occurs on the border of the dip equator [*Paranicas and Cheng*, 1994, Figure 4]; since the drift path surface is essentially a minimum B surface for energetic particles, the converging drift paths of 90° pitch angle particles into the planetary surface might provide an alternative explanation for some of the UV emissions observed by the Voyager 2 (emission regions 1, 2, and 5 designated by *Paranicas and Cheng* [1994], also discussed by *Ho et al.* [1997]).

The three regions indicated in Plate 2 correspond to a similar section of the minimum B contours which *Acuña et al.* [1993] calculated for 90° pitch angle particle drift shell. They found no solution for a broad section (30°–180°W) of the minimum B contours and concluded that particles which drift into this region will precipitate into the atmosphere. Our results show that the precipitation is possible everywhere along the magnetic dip equator, since the minimum B surface (in our case maximum μ surface to be exact) intercepts the planet's surface. This is true, of course, only for the special case of $J = 0$ particles. In general, $J \neq 0$ particles bounce along the field lines and precipitate into the atmosphere at the field line footpoints, giving rise to types of UV emissions from regions on the planetary surface where drift shells collapse [*Ho et al.*, 1997].

The zero second adiabatic invariant particles might play a more significant role than first appears. First, particles of pitch angle less than 90° would be lost at the ends of the field line in less than one bounce motion at this short distance from the planet; second, 90° pitch angle particles drift more or less on the same surface (min B) for a large range of energies as long as the kinetic energies are large enough for the gradient drift to dominate. The consequence is that particles with a large range of energies enter the atmosphere along the magnetic equator. *Gao et al.* [this issue] found that at Uranus the $J = 0$ particles drift into the planetary surface at regions coinciding with some of the weak UV emissions [*Herbert and Sandel*, 1994], which provides good evidence that precipitation into the magnetic equator of this type of particles does occur.

Figure 7 shows the magnitude of the drift velocities plotted against the radial distance at about 180°W for particles of several energies. For energetic particles, the drift velocity is basically a function of their kinetic energies, and the gravitational and centrifugal drift are negligible in comparison. Drift velocities of 1 eV particles are typically less than a few m/s. Imposed on these drift velocities is also the solar wind driven **E**×**B** drift (dashed line) calculated from (4). The magnitudes of two drift velocities are comparable for ions having energy of roughly 100 eV at 2 R_N. Since their directions are opposite, the two drifts are approximately canceled out at that distance.

The drift velocities of low energy particles, however, are strongly affected by gravity and centrifugal force and, as such, are highly asymmetric due to the large tilted angle of the dipole axis. The asymmetric plasma density distribution and drift velocity imply a complicated drift current inside the plasmasphere of Neptune. (One such asymmetric drift pattern can be found in Plate 3 of *Gao et al.* [this issue] for particle drift in the Uranian magnetosphere.) Particles of total energy –3.2 eV have kinetic energies ranging from about 1 eV near the planet's surface to about 0.5 eV at $r \sim 4.5\ R_N$. At this low energy, the drift velocities at about 4 R_N range from 0.02 m/s to 4 times that, and they drop by a factor of 10 at a distance very near the planetary surface. The smallness of the drift velocities means that the drift of particles into the planetary surface will not affect the formation of the plasmasphere.

5. Discussion and Conclusions

Based on the fact that the refilling time of the ionospheric ions is less than the solar wind driven convection time within a few planetary radii, we set out to argue for the existence of a plasmasphere at Neptune and proceeded to estimate its size, density, and temperature. The existence of a plasmasphere at Neptune is supported by the fact that Voyager 2 PWS detected large dispersive Whistler waves, suggesting large densities along field lines. Other evidence is the lack of report on the day-night asymmetries in plasma density. Such density asymmetries have been used as an argument for a convection-dominated magnetosphere at Uranus. In the case of Uranus, convection domination, and hence the lack of a plasmasphere, may be supported by the theoretical argument that solar wind particles can penetrate easily into the inner magnetosphere because of the near alignment of the spin axis and the solar wind flow. The penetration, however, may not be achieved so readily if the inner flux tubes are filled by interhemispherical plasma flow in a timescale that is short compared to the convection time. In fact, sharp plasma edges were observed at Uranus which may be explained by the reduction of the electric field in the inner region that thus provides some sort of "shielding" [*Wolf*, 1983]. The method used in this paper can be applied to Uranus to determine if it has a plasmasphere.

In the first approximation, the plasma was assumed to be in an equilibrium state, and the boundary at which the plasma refilling time equals the solar wind driven convection time is taken to be the plasmapause. The plasmasphere so obtained has a size of about 7 planetary radii on the zero magnetic scalar potential surface, which is obviously overestimated, indicating an equilibrium state of plasmaspheric plasma to be a poor assumption.

In more accurate calculations, we have taken the effect of accessibility of ions from the ionosphere to a certain point on a field line due to both the potential barrier resulting from the gravity and centrifugal force and the requirement of the local refilling time to be less than the solar wind driven convection time. By calculating the time to fill a flux tube from the ionosphere to a specific point on the field line for the ions which are able to cross the potential barriers and comparing with the convection time, the accessibility of the ionospheric ions of various speeds to

that particular point was determined. The density and temperature of the plasma at the local point were then obtained by integrating over all the ions that are accessible to the concerned point. By this we found that Neptune has a plasmasphere which has its boundary located between 3.25 and 4.5 R_N on the zero magnetic scalar potential surface.

The calculated H^+ densities and temperatures were compared with the Voyager 2 observations. The measured density minima at about 3 R_N inbound and 5 R_N outbound were roughly the location of the plasmapause we calculated. The plasma density drops exponentially with distance inside the plasmasphere because of the large gravity of Neptune, and the sudden density drop-offs at the plasmapause we calculated have magnitudes a few orders lower than the ionospheric density. The Neptunian plasmasphere is therefore quite different from Earth's plasmasphere, which has a density that does not decrease appreciably with distance until the drop-off at the plasmapause. The high temperatures observed may result from the high-speed tails of the ions escaping from the ionosphere. Other sources of plasmas such as solar wind particles and plasmas originating from Neptune's moons and rings, as well as various heating processes, may also contribute to the measured bulk plasma parameters.

We also calculated the particle drifts. Only 90° pitch angle particles are considered in this paper, which simplifies the problem to two-dimensions by removing bounce motions. Due to the high nondipole magnetic components, particles very near the planet do not execute complete 360° drifts, similar to *Acuña et al.*'s [1993] results given on the minimum B contours. Energetic 90° pitch angle particles precipitate into the atmosphere along the magnetic equator on the planetary surface, providing an alternate explanation for *Paranicas and Cheng*'s [1994] "monoprecipitation." In the range of 2 – 4 R_N, particles of energies of 100 eV and above drift at the speeds that are comparable to the solar wind driven convection speeds, of the order of a few m/s. The drifts of particles of lower energies are strongly affected by the gravitational and centrifugal forces, and constrained to the surfaces where the first invariant of the particles is maximum on each field line.

Acknowledgments. This work is supported by NASA grant NAG5-2317. The authors express their thanks to John Richardson for providing the Voyager PLS ion data for figures 5 and 6, and to Jack Connerney for the Voyager 2 trajectory coordinates.

References

Acuña, M. H., J .E. P. Connerney, and N. F. Ness, Neptune's magnetic field: Calculation of field geometric invariants derived from the I8E1 GSFC/BRI model, *J. Geophys. Res.*, *98*, 11,275, 1993.

Brice, N. M., Bulk motion of the magnetosphere, *J. Geophys. Res.*, *72*, 5193, 1967.

Connerney, J. E. P., M. H. Acuña, and N. F. Ness, The magnetic field of Neptune, *J. Geophys. Res.*, *96*, 19,023, 1991.

Gao, S., C. W. Ho, T. S. Huang and C. Alexander, Uranus' magnetic field and particle drifts in its inner magnetosphere, *J. Geophys. Res.*, this issue.

Gurnett, D. A., W. S. Kurth, R. L. Poynter, L. J. Granroth, I. H. Cairns, W. M. Macek, S. L. Moses, F. V. Coroniti, C. F. Kennel, and D. D. Barbosa, First plasma wave observations at Neptune, *Science*, *246*, 1494, 1989.

Herbert, F., and B. R. Sandel, The Uranian aurora and its relationship to the magnetosphere, *J. Geophys. Res.*, *99*, 4143, 1994.

Ho, C. W., T. S. Huang, and S. Gao, Contributions of the high degree multipoles of Neptune's magnetic field: A Euler potentials approach, *J. Geophys. Res.*, *102*, 24,393, 1997.

Huang, T. S., and T. J. Birmingham, The polarization electric field and its effects in an anisotropic rotating magnetospheric plasma, *J. Geophys. Res.*, *97*, 1511, 1992.

Kavanagh, L. D., Jr., J. W. Freeman Jr., and A. J. Chen, Plasma flow in the magnetosphere, *J. Geophys. Res.*, *73*, 5511, 1968.

Lemaire, J., The "Roche-limit" of ionospheric plasma and the formation of the plasmapause, *Planet. Space Sci.*, 22,757, 1974.

Lemaire, J., *Frontiers of the Plasmasphere*, pp. 209-210, Institut d'Aeronomie Spatiale de Belgique, Brussel, Belgium, 1985.

Lemaire, J., Plasma distribution models in a rotating magnetic dipole and refilling of plasmaspheric flux tubes, *Phys. Fluids B*, 1, 1519, 1989.

McNutt, R. L., Jr., R. S. Selesnick, J. D. Richardson, Low-energy plasma observations in the magnetosphere of Uranus, *J. Geophys. Res.*, *92*, 4399, 1987.

Ness, N. F., M. H. Acuña, L. F. Burlaga, J. E. P. Connerney, R. P. Lepping and F. M. Neubauer, Magnetic fields at Neptune, *Science*, *246*, 1473, 1989.

Nishida, A., Formation of plasmapause, or magnetospheric plasma knee, by the combined action of magnetospheric convection and plasma escape from the tail, *J. Geophys. Res.*, *71*, 5669, 1966.

Paranicas, C., and A. F. Cheng, Drift shells and aurora computed using the O8 magnetic field model for Neptune, *J. Geophys. Res.*, *99*, 19,433, 1994.

Richardson, J. D., J. W. Belcher, M. Zhang, and R. L. McNutt Jr., Low-energy ions near Neptune, *J. Geophys. Res.*, *96*, 18,993, 1991.

Selesnick, R. S., Plasma convection in Neptune's magnetospheres, *Geophys. Res. Lett.*, *17*, 1681, 1990.

Selesnick, R. S., and J. D. Richardson, Plasmasphere formation in arbitrarily oriented magnetospheres, *Geophys. Res. Lett.*, *13*, 624, 1986.

Tyler, G. L., et al., Voyager radio science observations of Neptune and Triton, *Science*, *246*, 1466, 1989.

Vasyliunas, V. M., The convection-dominated magnetosphere of Uranus, *Geophys. Res. Lett.*, *13*, 621, 1986.

Wilson, G. R., J. L. Horwitz, and J. Lin, A semikinetic model for early stage plasmasphere refilling, 1, Effects of Coulomb collisions, *J. Geophys. Res.*, *97*, 1109, 1992.

Wolf, R. A., The quasi-static (slow-flow) region of the magnetosphere, in *Solar-Terrestrial Physics*, edited by R. L. Carovillano and J. M. Forbes, pp. 303-368, D. Reidel, Norwell, Mass., 1983.

Figure Captions

Plate 1a. Color contours of the equilibrium ionosphere-originated H^+ density on four surfaces of constant β. The solid white lines are magnetic field lines. Contours of α (closed rings) and β (radial lines) on the zero magnetic scalar potential surface are marked as black lines. The x, y, and z axes are the same as the planetary rotation frame shown in Figure 1.

Plate 1b. Color contours of the equilibrium ionosphere-originated H^+ density on the zero magnetic scalar equipotential surface. The boundaries of the plasmasphere are marked with crosses for the case of a "pole-on" orientation (minimum solar wind and inner magnetosphere convection coupling), and with circles for the case in which the solar wind flow direction is perpendicular to the dipole axis (maximum coupling). The inner boundary (asterisks) is for the case of dynamic accessibility of the ions when comparison of the convection time and the ion speed dependent refilling time is considered. The white lines are the same contours of α and β as in Plate 1a.

Plate 2. Drift paths of ions of total energy 1 eV. The regions marked I, II, and III are locations where drift ions are likely to enter the atmosphere. The region (marked by **O** adjacent to it) is a result of the distorted magnetic configuration due to the high nondipole magnetic components. Particle drifts at this energy are strongly affected by the gravitational and centrifugal forces.

Figure 1. Relative orientations of Neptune's rotation axis $\boldsymbol{\Omega}$, dipole axis **M**, and solar wind flow direction $\mathbf{v}_{SW}$ The solar wind vector $\mathbf{v}_{SW}$ rotates about $\boldsymbol{\Omega}$ with time t in a rotation frame in which **M** is fixed. The x axis is in the plane of Neptune's 0 degree planetary longitude, and y axis is along the 270°W longitude using the Neptune longitude system (NLS) adopted by the Voyager Project Steering Group. The dipole tilted polar angle θ_D and the dipole azimuthal offset angle ϕ_D are 47° and 18°, respectively. The angle between the solar wind flow direction and the spin axis θ_S is 67°.

Figure 2. Potential energies on the zero magnetic scalar potential surface plotted versus radial distances: gravitational (crosses), centrifugal (triangles), gravitational and centrifugal (circles), polarization electrical (squares), and total potentials (thick line). The densities are also shown (thin line).

Figure 3. H^+ density (thin line) and temperature (thick line) along a field line at about 0°W at the equilibrium state plotted against the Neptunographic latitude. Overplotted are the density (squares) and temperature (crosses) of ions that are able to cross the potential barriers P1 and P2. The potential trough is marked by T, and the maximum radial distance reached by the field line is roughly at 8 R_N indicated by the solid circle.

Figure 4. Refilling time plotted versus ion speed according to (12). Cases A-1 to A-3 are cases in which the refilling time t at the cutoff speed is shorter than the local convection time t_c. Cases B-1 and B-2 are for $t > t_c$ at the minimum cutoff speed. A-1 represents the case in which all ions that have crossed the potential barrier can reach the local point. A-2, A-3, and B-1 are cases mostly likely found in the plasmapause. The high-speed tail might be responsible for the high temperatures observed.

Figure 5. Comparison of Voyager 2 PLS measured H^+ densities with the calculated results. The calculated results are shown for the equilibrium state case (squares), the case in which ions can cross over the potential barriers (circles), and the case in which ions have the speed dependent refilling time less than the convection time (triangles). The open and solid triangles correspond to Cases A-2 and A-3 of Figure 4.

Figure 6. Comparison of Voyager 2 PLS measured H^+ temperatures on its inbound and outbound trajectory with the calculated results. The circles mark the temperatures calculated when

only the ions that can cross the potential barriers are considered. The triangles mark the temperatures calculated from only the high-speed tails of the distribution function of the ions that have the speed dependent refilling time less than the convection time.

Figure 7. Ion drift speed as a function of the radial distance. Ions of energy about 100 eV have a magnitude of drift speed comparable to the solar wind driven convection drift (dashed line).

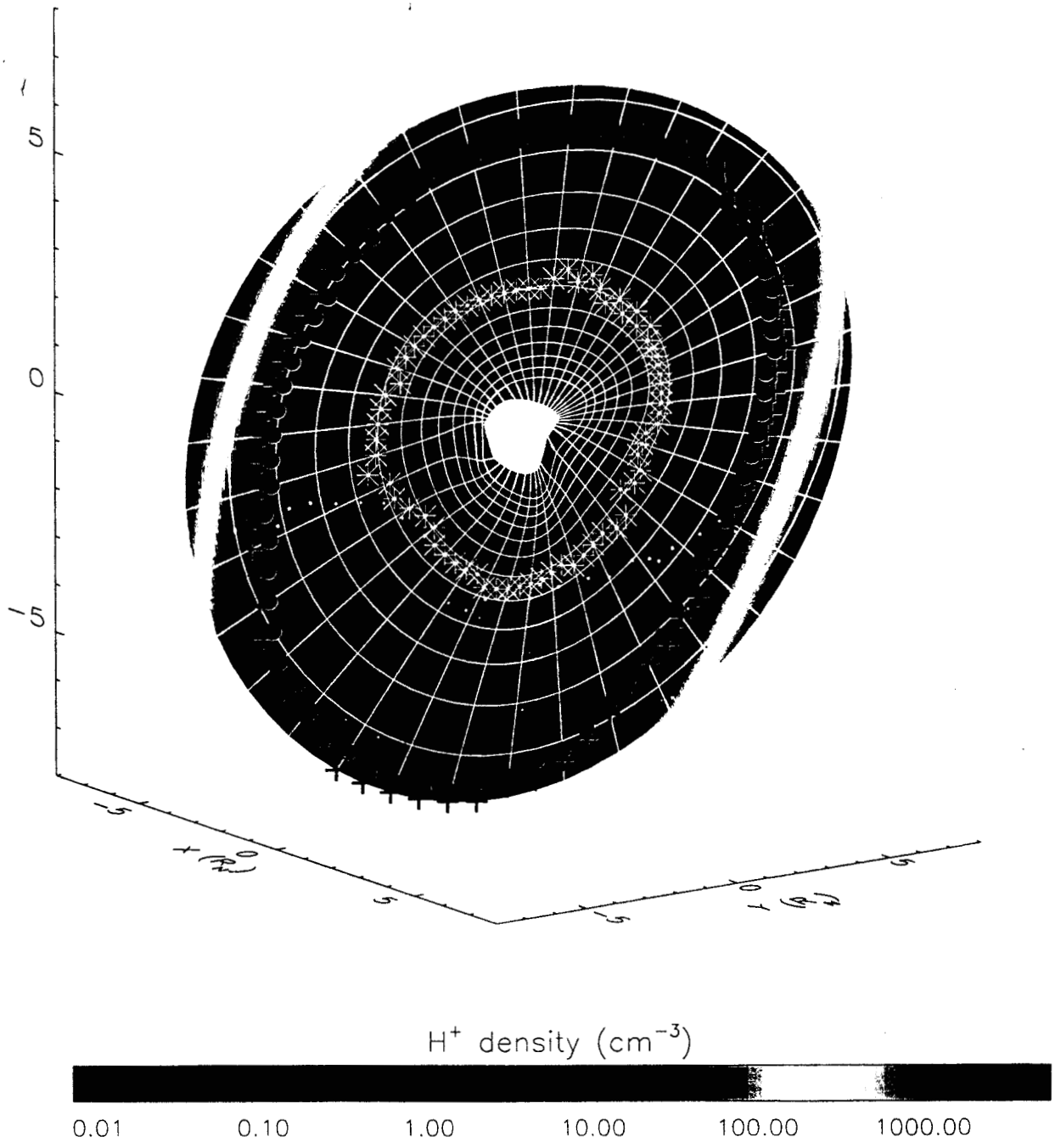

Plate 1b

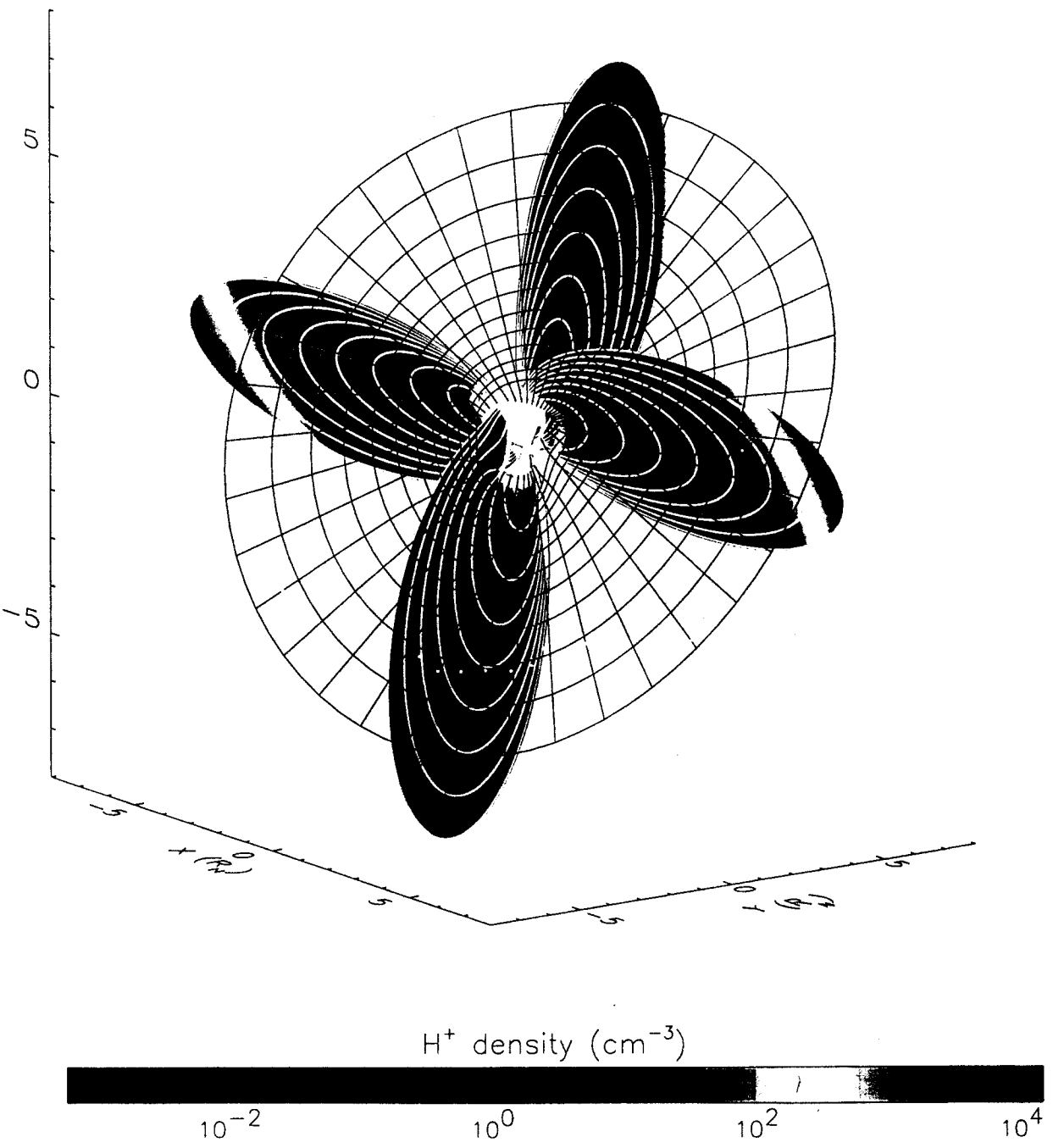

Plate 1a

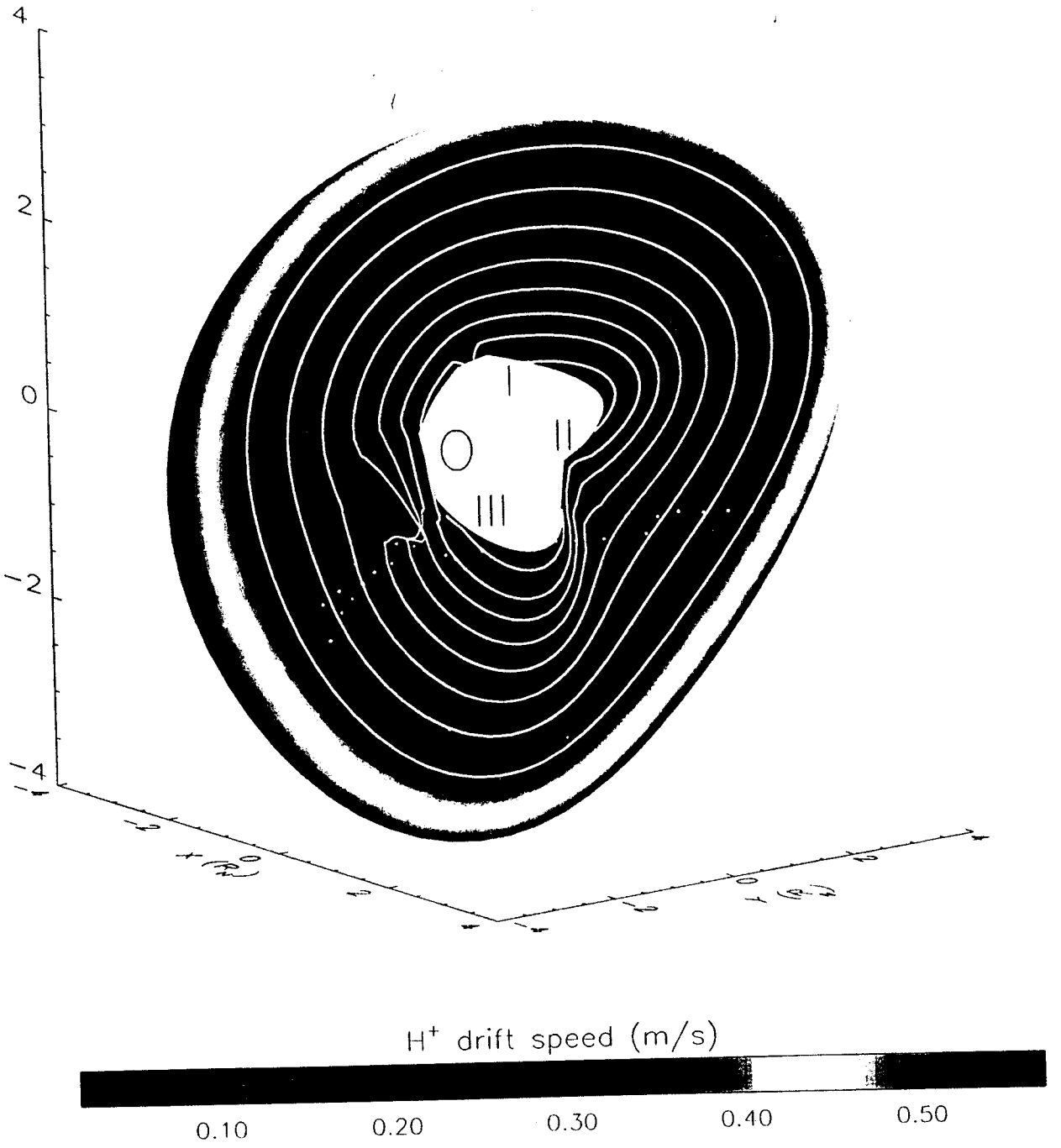
4
2
0
−2
−4
I
II
III
H+ drift speed (m/s)
0.10
0.20
0.30
0.40
0.50

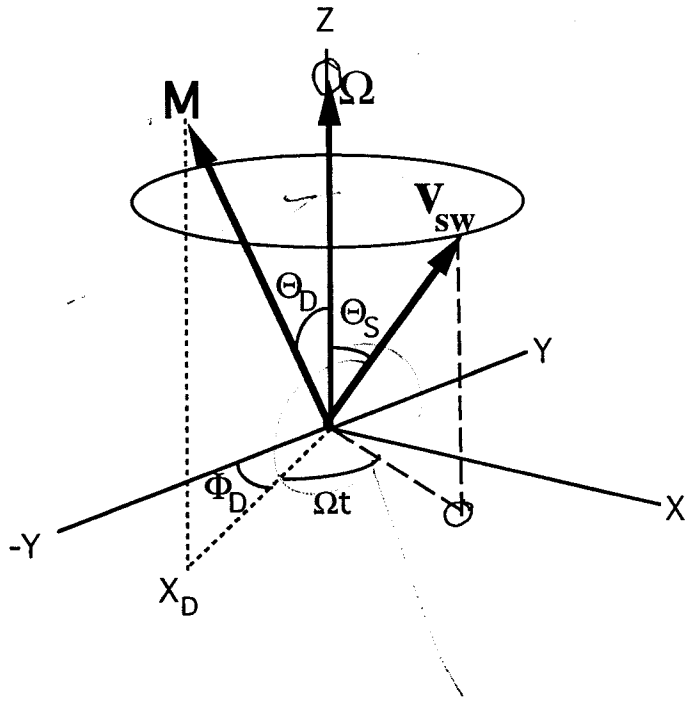

Fig 1

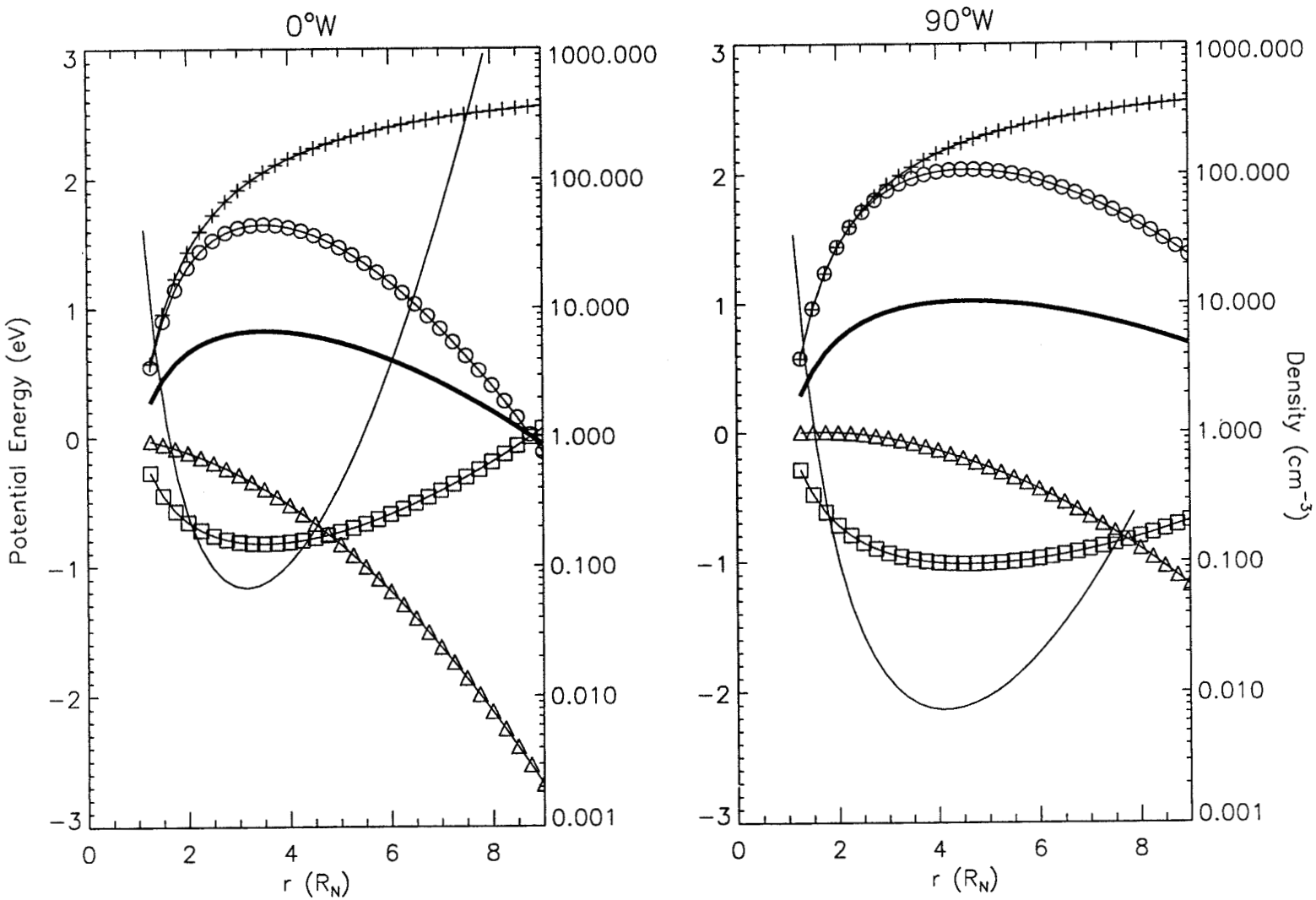
0°W
90°W
Potential Energy (eV)
Density (cm^{-3})
r (R_N)
3
2
1
0
−1
−2
−3
0
2
4
6
8
1000.000
100.000
10.000
1.000
0.100
0.010
0.001

Figure 2

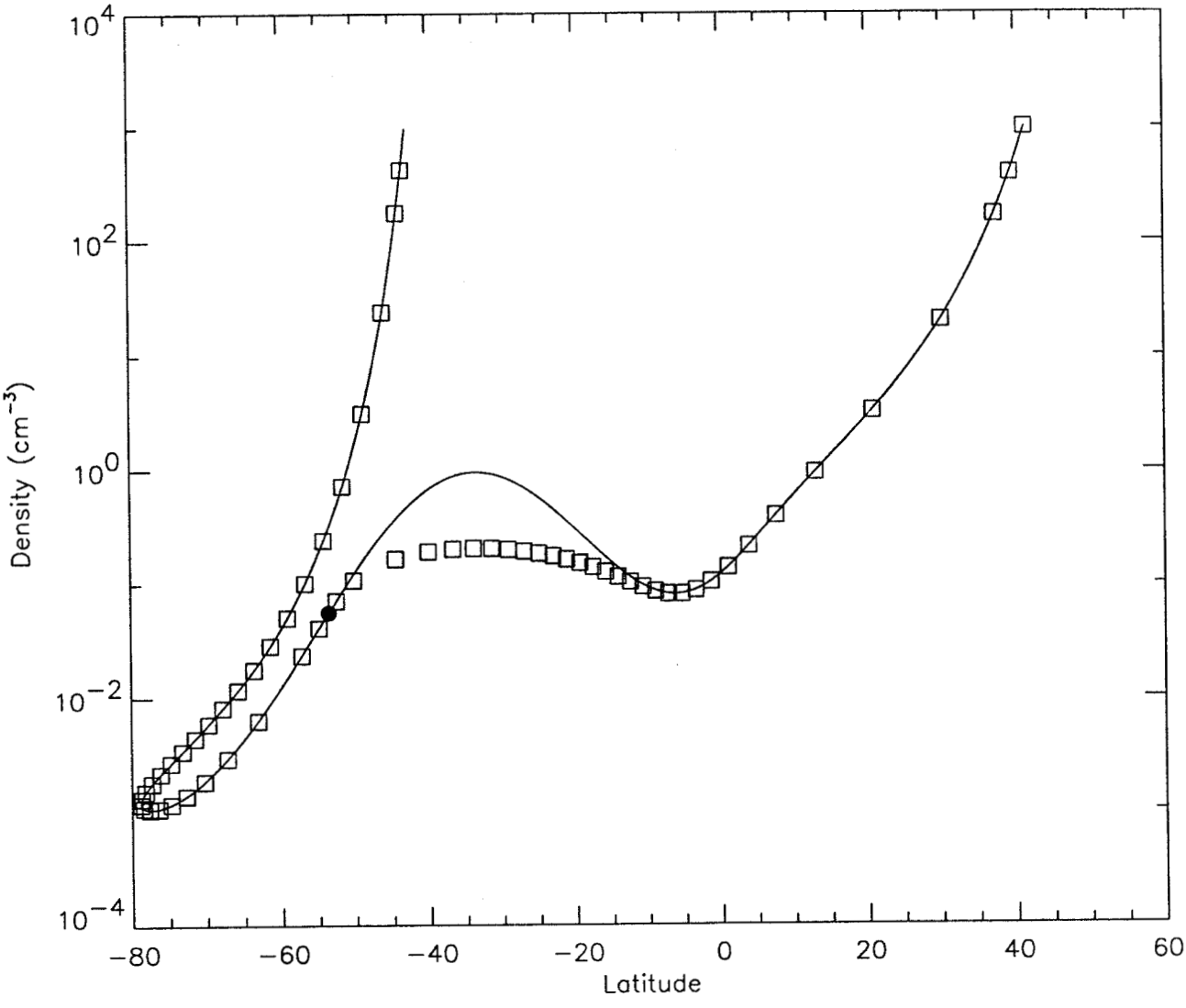

Figure 3

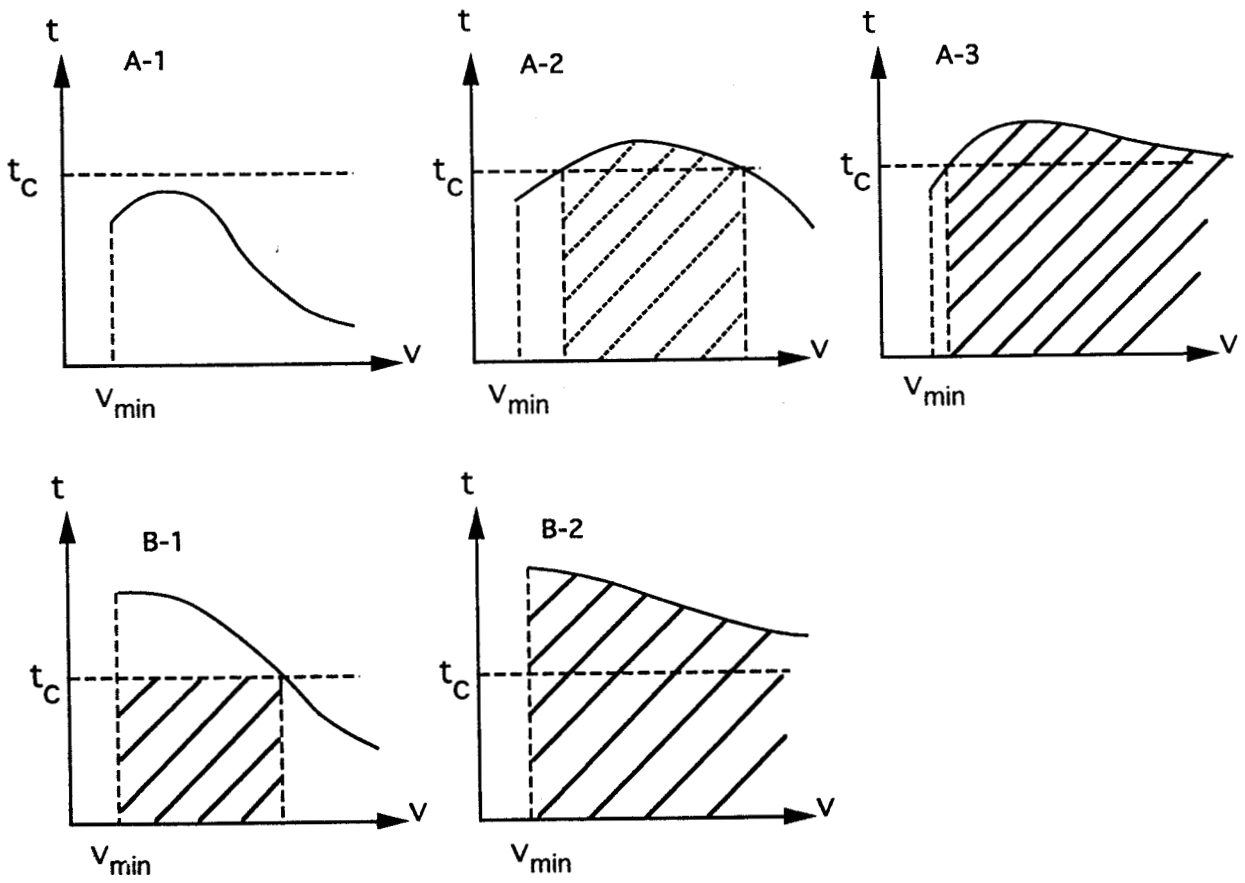
t
A-1
t_c
V
V_{min}
t
A-2
t_c
V
V_{min}
t
A-3
t_c
V
V_{min}
t
B-1
t_c
V
V_{min}
t
B-2
t_c
V
V_{min}

Figure 4

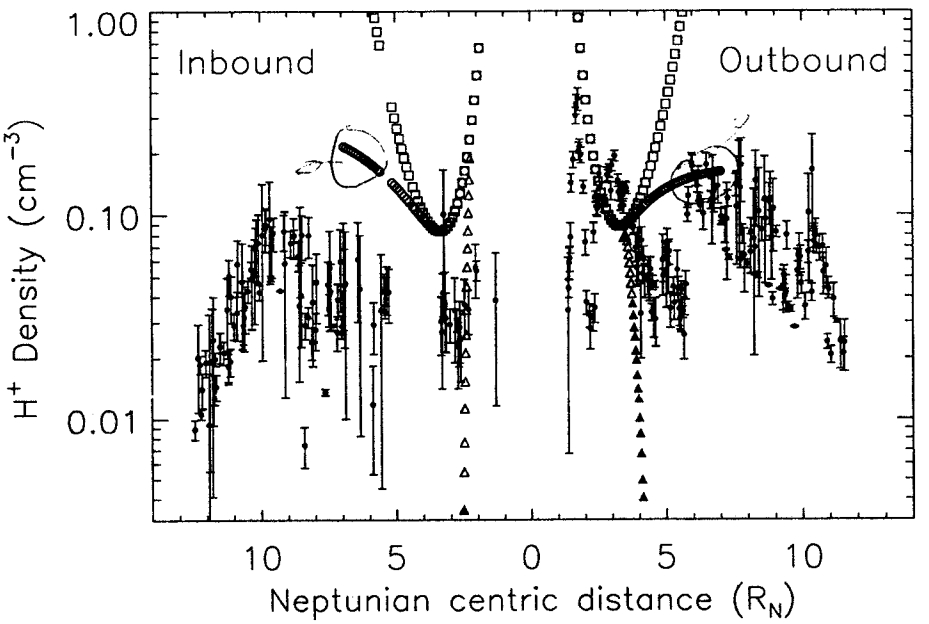
1.00
0.10
0.01
Inbound
Outbound
H+ Density (cm-3)
10
5
0
5
10
Neptunian centric distance (RN)

Figure 5

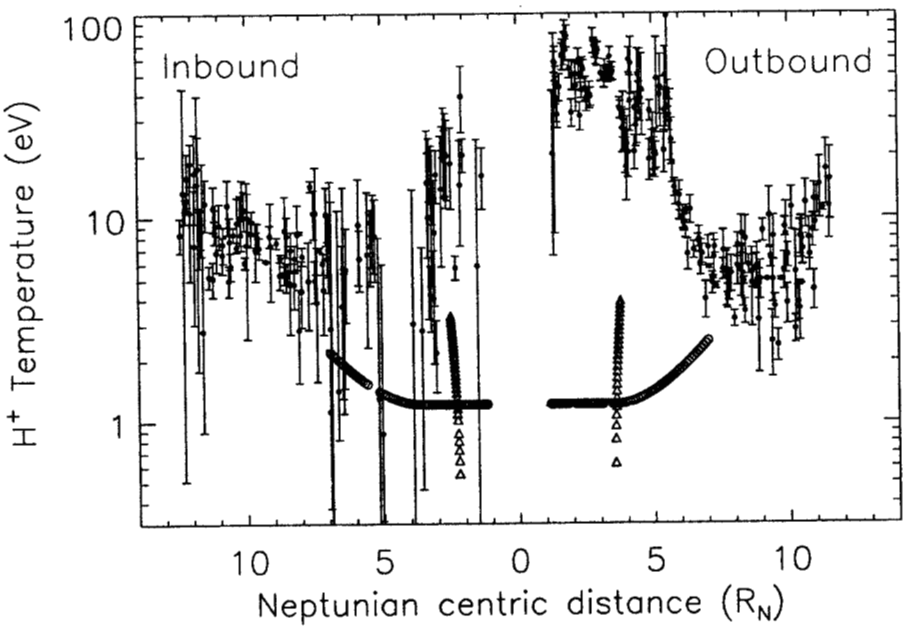
100
10
1
Inbound
Outbound
H+ Temperature (eV)
10
5
0
5
10
Neptunian centric distance (RN)

Figure 6

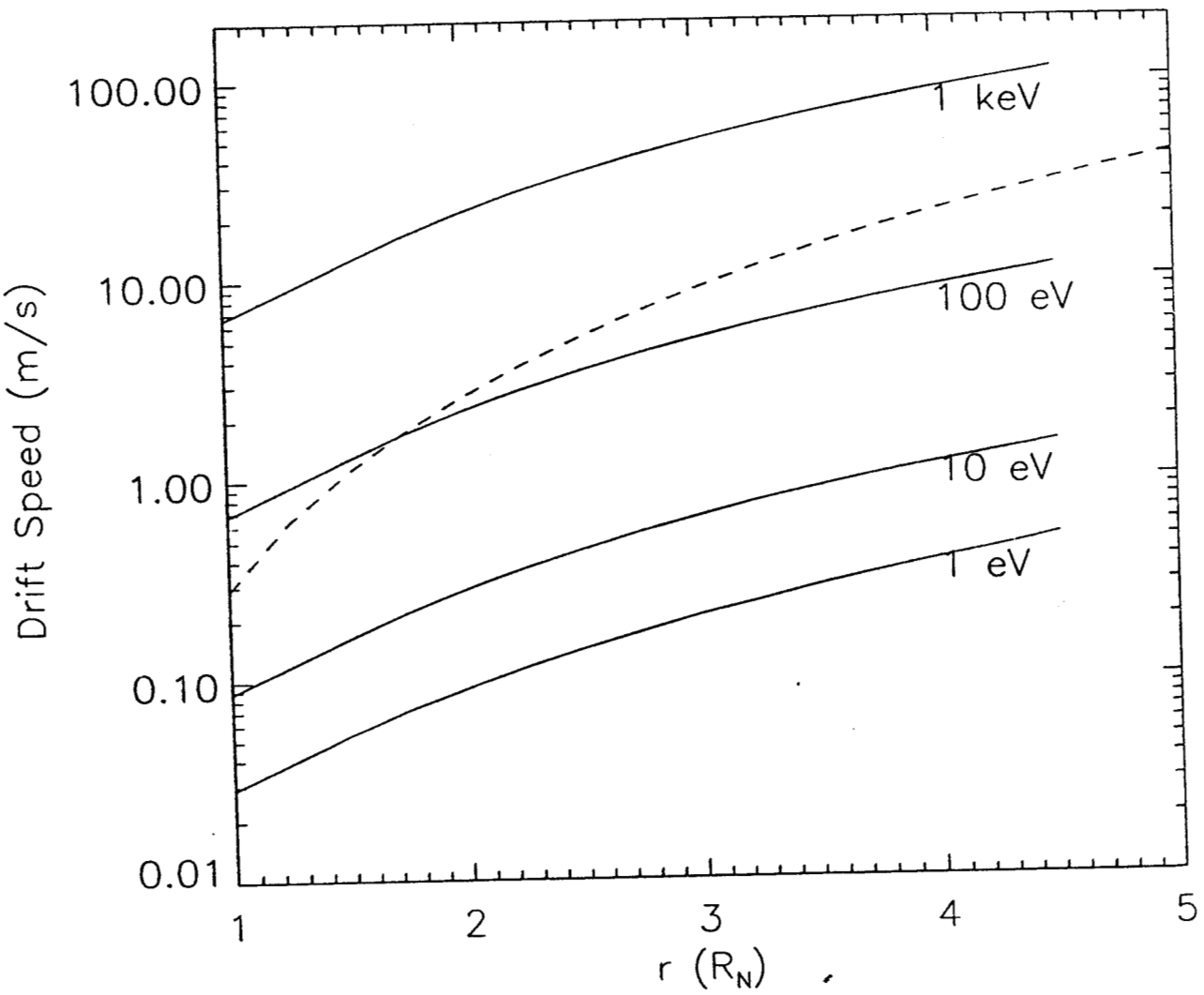
100.00
10.00
1.00
0.10
0.01
Drift Speed (m/s)
1 keV
100 eV
10 eV
1 eV
1
2
3
4
5
r (R_N)

Figure 7